Author Manuscript

Author Manuscript

Author Manuscript

Author Manuscript

HHS Public Access

Author manuscript

Magn Reson Imaging Clin N Am. Author manuscript; available in PMC 2020 February 01.

Published in final edited form as:

Magn Reson Imaging Clin N Am. 2019 February ; 27(1): 1–13. doi:10.1016/j.mric.2018.08.005.

Radiomics in Kidney Cancer: Magnetic Resonance Imaging

Alberto Diaz de Leon, M.D., [Assistant Professor of Radiology],
University of Texas Southwestern Medical Center. Dallas, TX

Payal Kapur, M.D., [Associate Professor of Pathology and Urology], and
Co-leader, Kidney Cancer Program, Harold C. Simmons Comprehensive Cancer Center. University of Texas Southwestern Medical Center. Dallas, TX

Ivan Pedrosa, MD, PhD* **[Professor of Radiology, Urology]**
Advanced Imaging Research Center, and Biomedical Engineering. Chief of MRI. Co-leader, Kidney Cancer Program, Harold C. Simmons Comprehensive Cancer Center. University of Texas Southwestern Medical Center. Dallas, TX

Synopsis:

Renal tumors encompass heterogeneous disease spectrum, which confounds patient management and treatment. Percutaneous biopsy is an invasive procedure with excellent accuracy for the diagnosis of kidney cancer, though limited by the inability to sample every part of the tumor at multiple time points, potentially limiting the accurate characterization of heterogeneous renal masses and detection of tumor changes over time. Imaging, particularly with quantitative magnetic resonance imaging (MRI), provides a noninvasive method for the detailed assessment of kidney tumors. In conjunction with Radiomics, imaging may provide detail beyond what can be achieved from human interpretation alone, including detailed insight into tumor biology. Understanding what these technologies can offer will allow radiologists to play a larger role in the care of patients with RCC. In this article, we review the use of radiomics in renal cell carcinoma, in both the pre-treatment assessment of renal masses and posttreatment evaluation of RCC, with special emphasis on the use of mpMRI datasets.

Keywords

Radiomics; kidney cancer; MRI; Quantitative Imaging

Introduction

Renal tumors encompass a broad disease spectrum including benign and indolent lesions to aggressive and invasive malignancies. Imaging plays a critical role in the management of patients with renal tumors. Small renal masses (SRMs), defined as ≤ 4 cm in size, account

*Corresponding author: Ivan Pedrosa MD, PhD, 2201 Inwood Rd. 2nd Floor, Suite 202, Dallas, TX 75390-9085 Phone: 214-645-2285, ivan.pedrosa@UTSouthwestern.edu.

Publisher's Disclaimer: This is a PDF file of an unedited manuscript that has been accepted for publication. As a service to our customers we are providing this early version of the manuscript. The manuscript will undergo copyediting, typesetting, and review of the resulting proof before it is published in its final citable form. Please note that during the production process errors may be discovered which could affect the content, and all legal disclaimers that apply to the journal pertain.

Author Manuscript Author Manuscript Author Manuscript Author Manuscript

for greater than 50% of all renal masses with approximately 20% of these demonstrating malignant behavior [1]. The American Urological Association guidelines for management of renal masses contemplate active surveillance (AS) as a valid option for patients with comorbidities and T1a (≤4cm) or T1b (4–7 cm) tumors. The ability to predict the histology of these renal lesions to distinguish aggressive forms of renal cell carcinoma (RCC) from benign and indolent malignant lesions with imaging has been a primary topic of interest. Furthermore, despite the reported low risk of metastases in larger tumors (i.e. cT1b/T2, >4 cm) followed on AS, the lack of reliable predictors of oncologic behavior and low reliability of biopsies to grade larger, heterogeneous tumors limit the applicability of AS in clinical practice for these tumors. Moreover, there is currently not accepted neoadjuvant therapy regimen in the management of kidney cancer. The inherent heterogeneous nature of renal tumors [2,3] drives the need to better characterize the disease and overcome the sampling variability of percutaneous biopsies. Imaging provides a whole-tumor assessment that has the potential to help select effective therapies for specific histologic subtypes. Nevertheless, the known histologic and molecular heterogeneity within the subtypes of RCC, and even within a single tumor, is such that the development of reliable imaging biomarkers to predict the histology and biologic behavior of these lesions is challenging.

Radiomics is an emerging field, which attempts to extract data from imaging to provide information beyond what can be achieved from human imaging interpretation alone. The correlation of these imaging data with genomics (i.e. radiogenomics), metabolomics (i.e. radiometabolomics), and beyond, offers an opportunity to generate objective, quantitative biomarkers of tumor biology that may be used to predict patient's prognosis and likelihood to response to therapy, overcoming some of the challenges associated to disease heterogeneity (Figure 1). Magnetic resonance imaging (MRI) provides rich imaging data sets because of the multiple image contrast mechanisms available with this technique (i.e. multiparametric MRI [mpMRI]). These datasets offer a unique opportunity to implement radiomic analysis. In this article, we review the use of radiomics in renal cell carcinoma, in both the pre-treatment assessment of renal masses and post-treatment evaluation of RCC, with special emphasis on the use of mpMRI datasets.

Radiomics Overview

Radiomics is a term that includes various techniques for the extraction of quantitative features from imaging to improve diagnostic, prognostic, and predictive accuracy of image interpretation. Gillies et al [4] define radiomics as "the conversion of images to higher dimensional data and the subsequent mining of these data for improved decision support". Radiomics approaches provide a mechanism to identify complex patterns in images that are not obvious to the naked eye. The recent breakthroughs in artificial intelligence (AI) and computer power have accelerated the application of this type of analysis to medical imaging to guide clinical decisions [5].

The process begins with selection and standardization of an imaging protocol. Uniformity in image acquisition is vital in any radiomics assessment to reduce variability and improve the reproducibility and comparability of studies. Mackin et al [6] reported a similar level of variability in the values of radiomics features calculated on computed tomography (CT)

Author Manuscript Author Manuscript Author Manuscript Author Manuscript

images obtained from different CT scanners to that of the variability of these radiomics features found in CT images of patients with non small cell lung cancers. In MRI, standardization of image acquisition may represent even a greater challenge due to the interplay of numerous factors including hardware (i.e. magnet strength, coil selection, etc.), sequence parameters, and contrast agents. For example, with dynamic contrast-enhanced (DCE) MRI, the type and dose contrast agent, software used to extract the pharmacokinetic parameters, and pulse sequence utilized for image acquisition must be accounted for [7]. Nevertheless, several organizations have attempted to introduce standardization of imaging techniques for quantitative analyses, such as the Quantitative Imaging Biomarkers Alliance [8].

Once an appropriate imaging protocol is selected, a volume of interest is identified. Depending on the prediction target, analyses can be performed on an entire lesion, metastases, and/or normal tissues. Additionally, analyses may be performed on subvolumes of tumor known as habitats, regions that may exhibit unique physiologic characteristics from the remainder of the tumor [9]. Volume of interests are then segmented, either manually or automatically, to determine which voxels are analyzed.

Segmentation is considered a critical component of radiomics, as the subsequent features data is generated from the segmented volumes. Manual segmentation is considered as ground truth, but is labor intensive, may not be feasible with large volumes of data, and suffers from inter-operator variability [10]. Semi-automatic segmentation methods, such as region-growing and level set methods, may maximize outputs and provide greater reproducibility, though still require some level of manual input by the operator. The method of segmentation can also affect the radiomic analysis [11]. Once the volumes are segmented, feature extraction can then be performed.

Feature extraction involves the mining of quantitatively attributes from the segmented volumes and encompasses the center of radiomics. The number of radiomic features that can be extracted is essentially limitless and requires careful selection, as inclusion of many features could result in overfitting. Predictive and prognostic radiomic features should be extracted from training sets and validated in independent datasets, when possible, to diminish the opportunity of overfitting. Features can be subdivided into two broad categories: semantic and agnostic features [4] Semantic features including descriptors commonly used in image interpretation by the radiologist, such as lesion shape, margin, and location. Agnostic features are those mathematically extracted from the image and be further subdivided into first-, second-, and higher-order statistical outputs [12].

First-order statistics are obtained from the histogram of voxel intensities to provide characteristics such as mean, skewness/asymmetry, kurtosis/sharpness, and measures of randomness, including entropy and uniformity. Firstorder features describe the distribution of intensities without taking into account the spatial relationship of voxels. Second-order, or texture or greyscale features, are based on matrices depicting spatial intensity distribution and describe the relationship between voxels with similar or different intensity values and can provide a measurement of intratumoral heterogeneity. Examples of these include gray-level co-occurrence matrix (GLCM) (Figure 2) and runlength matrix [12]. Haralick first

Author Manuscript Author Manuscript Author Manuscript Author Manuscript

described a series of texture features commonly applied to medical imaging (Box 1)[13]. Finally, higher-order statistical outputs employ filters grids on the image to identify repetitive or nonrepetitive patterns.

Ultimately, the goal of radiomics is to use imaging features to identify patterns which can be used individually or correlated with patient characteristics beyond imaging (e.g. histology, immunohistochemistry, genomic and proteomic profiles, etc.) to generate objective, quantitative biomarkers of disease status that can improve diagnosis, inform on patient prognosis, and predict response to therapy. This requirement for expansive data sets mandates the creation of large databases through which data may be mined and patterns may be discovered. An intermediate step toward the described radiomic analysis is the use of quantitative MRI techniques for characterization of disease aggressiveness in kidney cancer. Understanding the correlation between these quantitative techniques and histopathologic, metabolic, and genetic conditions will facilitate the implementation of radiomic analyses. Here we discuss some of these techniques for evaluation of patients with renal masses in general, localized kidney cancer, and locally advanced and/or metastatic kidney cancer.

Radiomics in the Pre-treatment assessment of renal masses

Intratumor heterogeneity presents a challenge in the preoperative assessment of renal masses. Percutaneous biopsy is an invasive procedure with excellent accuracy for the diagnosis of kidney cancer. However, biopsies are limited by the inability to sample every part of the tumor at multiple time points, potentially limiting the accurate characterization of renal masses (ie. subtyping, tumor grading). MRI is well-suited for a comprehensive evaluation of renal masses, particularly with its ability to provide quantitative and functional assessments, such as diffusion-weighted imaging (DWI), arterial spin labeling (ASL), and dynamic contrast enhancement (DCE). MRI may also be utilized at multiple time points without the drawback of radiation exposure, allowing renal masses to be followed over time to detect changes in lesion characteristics which may reflect changes in tumor histology and aggressiveness.

Radiomics for Subtyping of renal masses

The noninvasive characterization of renal masses using qualitative features on MRI has been well-described [14–16]. The more common subtypes of renal cell carcinoma can be differentiated primarily using a combination of T2-weighted and post-contrast imaging. Clear cell renal cell carcinoma (ccRCC), the most common and aggressive subtype, most often exhibits hyperintense signal on T2-weighted images and avid enhancement, in addition to intravoxel fat. On the other hand, papillary renal cell carcinoma (pRCC) tends to show hypointense signal on T2-weighted imaging and show low-level enhancement. Finally, chromophobe renal cell carcinoma (chrRCC) demonstrate variable signal intensity relative to renal parenchyma on T2-weighted images and show moderate enhancement.

Quantitative assessment of renal mass enhancement is not just an academic exercise. Indeed, there are several clinical scenarios where these measures can have substantial impact on patient management [17]. Therefore, attention to the acquisition technique and standardization across patients is important [18]. For example, a high arterial-to-delay enhancement ratio

Author Manuscript Author Manuscript Author Manuscript Author Manuscript

(>1.5) on multi-phasic contrast-enhanced MRI, combined with homogeneous low signal intensity on T2-weighted images, has a sensitivity of 73% and specificity of 99% in distinguishing an angiomyolipoma without visible fat (i.e. fat-poor angiomyolipoma [fpAML]) from RCC [19]. Quantification of contrast enhancement on multi-phasic contrast-enhanced MRI can play a complementary role to tissue biopsies in patients presenting with locally advanced and/or synchronous metastatic disease at diagnosis and can assist in the selection of optimal therapy for these patients (Figure 3).

Quantitative assessment with DWI may be of utility to assist with characterizing renal masses as well. Signal on DWI is dependent on the motion of water molecules in the extracellular space and provides a noninvasive assessment of tissue cellularity, integrity of cell membranes, and microcapillary perfusion. Overall, malignant solid renal masses are reported to demonstrate lower ADC values than benign lesions [20]. Using qualitative features alone, renal oncocytomas (RO) exhibit imaging features which may overlap with subtypes of RCC, particularly ccRCC and chrRCC. A meta-analysis of diffusion-weighted imaging of renal lesions, however, described ADC values for ROs tend to be higher (2 ± 0.08 × 10–3 mm2/s) than RCC (1.5 ± 0.08 ×10–3 mm2/s). For example, Taouli et al [21] reported significantly higher ADC values for ROs (mean ADC 1.91 ± 0.97 × 10–3 mm2/s) than solid RCCs (mean ADC 1.54 ± 0.69 × 10–3 mm2/s).

Nevertheless, absolute ADC values are affected by numerous factors and may vary between MR systems and field strengths. Histogram analyses may help overcome these limitations and provide a more reliable quantitative assessment, as distribution parameters are independent of signal intensity. A histogram analysis of DWI features may be used to differentiate benign from malignant neoplasms, as histogram-based assessment provides the benefit of quantitatively assessing the heterogeneity characteristically exhibited by ccRCC. Gaing et al [22] used whole lesion histogram analysis of intravoxel incoherent motion (IVIM) on renal lesions, and of the distribution parameters, kurtosis (i.e. a measure of flatness of the histogram) of the perfusion fraction was the only variable to distinguish RO from ccRCC. These authors also found the mean and standard deviation of tissue diffusivity and kurtosis of perfusion fraction could distinguish ccRCC from angiomyolipomas (AML). Histogram analysis of contrast enhancement patterns has also been used to differentiate among different renal masses as well. Chandarana et al [23] found the histogram distribution parameters of kurtosis and skewness on contrast enhanced MRI acquisitions to be significantly different between ccRCC and pRCC.

Textural analyses have also been used on computed tomography (CT) to predict histologic subtypes and grade. On portal venous phase images, entropy, a measure of histogram uniformity, and standard deviation correlate positively with ccRCC subtype on whole lesion analyses [24]. In the same study, an association between texture features and survival measures, including overall survival and time to disease recurrence, was seen with the histogram distribution parameters of standard deviation, mean, and entropy on unenhanced CT images. Global heterogeneity features, including run-length nonuniformity and gray-level nonuniformity, were significantly greater for sarcomatoid RCC tumors, an aggressive differentiation of RCC associated with a poor prognosis, when compared with non-sarcomatoid ccRCC [25].

Author Manuscript Author Manuscript Author Manuscript Author Manuscript

Future Role for Radiomics in Predicting Tumor Biology

Over the past decade, the incidence of incidentally detected renal masses has increased with the majority of those made up small renal masses (≤ 4 cm).[1] Approximately 20% of these masses are benign and many others exhibit an indolent growth pattern. In patients with comorbidities and increased surgical risk, active surveillance may be pursued as a management option. In this setting, the prediction of tumor grade within each specific subtype of renal cell carcinoma would be an essential part in the assessment of renal lesions. Furthermore, a method to further assess noninvasively changes in histopathologic and molecular tumor characteristics on subsequent follow-up imaging that predict a change in oncologic behavior would be of great value in managing these patients. As tumors undergo transformation from a low-grade neoplasm to a high-grade and aggressive tumor, detection of these changes would allow for early intervention before the tumor acquires the ability to metastasize or invade locally (Figure 4). This transformation is likely the result of changes in genetic and metabolic alterations, which are difficult to determine in clinical practice due to the impracticality of performing multiple serial biopsies, so a method to assess for this change non-invasively such as liquid biopsies or imaging would radically transform the management of patients undergoing active surveillance.

Ideally, such imaging methods would rely on robust, reproducible imaging techniques. The described variability of MRI protocols, sequences, and hardware challenge this concept. T2-weighted single-shot fast spin echo (SSFSE) acquisitions however, are known to be robust and reliable in most state-of-the-art MRI scanners and therefore, could be an optimal candidate for radiomics. Texture analysis of T2-weighted SSFSE images may be helpful in predicting tumor grade in clear cell renal cell carcinoma (Figure 5). Similarly, texture features on T2-weighted images have been shown to be predictive of molecular alterations in other tumors such as glioblastomas [26].

Quantitative MRI techniques have been explored to evaluate for imaging features that may correlate with histologic and metabolic features. Insight into the von Hippel-Lindau tumor suppressor gene (*VHL*) and its importance in regulation of the hypoxia pathway was revolutionary in understanding the tumor biology of ccRCC. Mutations/inactivation of *VHL* in the unregulated expression of hypoxia response elements and ultimately angiogenesis, which has been described to be associated with ccRCC prognosis and ability to metastasize [27,28]. An imaging technique that can estimate tumor microvascular density (MVD) may provide a noninvasive method to assess tumor angiogenesis and perhaps aggressiveness. ASL is one such potential technique, which uses arterial blood protons to assess tissue perfusion without the use of an exogenous contrast agent. Tumor perfusion estimated by ASL imaging has been shown to correlate with microvessel density on histopathology both in human samples and RCC xenografts [29–31]. In human studies of ccRCC, ASL was able to detect intratumoral heterogeneity within a single tumor by showing areas with different degrees of tissue perfusion, which correlate with differences in microvessel density and tumor cellularity on histologic assessment [30,32].

Multi-echo Dixon-based MRI, which uses a chemical shift technique to detect and quantify lipid, has been used as a noninvasive method to assess the metabolic features of ccRCC. Alterations in lipid metabolism result in the storage of lipids in intracytoplasmic vacuoles,

Author Manuscript Author Manuscript Author Manuscript Author Manuscript

characteristically manifested on imaging as decreased signal intensity on T1-weighted opposed-phase images relative to in-phase images. Furthermore, ccRCC expresses high levels of enzymes necessary to produce fatty acids and lipids, and two of these, fatty acid synthase (FASN) and stearoyl-CoA desaturase (SCD1), are associated with poor prognosis [33,34]. Multi-echo Dixon acquisitions with multi-peak fat spectral modeling provide a method to further quantify the presence of fat by providing a fat fraction (FF) – MRI signal arising from fat relative to the total MRI signal (i.e. fat plus water)[35]. Zhang et al [36] reported that FF quantification provided by Dixon MRI correlated with intracellular lipid at histopathology. ccRCCs showed heterogeneous accumulation of fat independent of tumor grade although the most aggressive tumors (ISUP grade 4/4) exhibited a statistical significant decrease in FF compared to grade 3 tumors. FF measures in ccRCC also correlated positively with triglyceride levels in tumor samples and negatively with phosphoethanolamine (PE), a predominantly membrane-localized lipid; the latter finding is consistent with previous reports suggesting that the PE pathway downregulation is another significant feature promoting growth in ccRCC [37].

Several studies have also described the use of ADC values to differentiate low-grade from high-grade ccRCC. Using an ADC cut-off of 1.20 × 10–3 mm2/s, one group reported a sensitivity and specificity of 0.65 and 0.96, respectively [38]; another group reported a sensitivity and specificity of 0.90 and 0.71, respectively, when using an ADC cut-off of 1.87 × 10–3 mm2/s.[39]

These MRI techniques may be of utility in patients on active surveillance where increases in tumor perfusion, changes in intratumor fat, and/or decrease in ADC may indicate evolution of the tumor toward a more aggressive phenotype. Better understanding of the correlation of MRI quantitative measures with histopathologic findings is crucial to adopt these biomarkers in the assessment of patients with renal masses (Figure 6).

Studies have also evaluated the use of quantitative and qualitative imaging features on CT to predict genetic mutations in renal cell carcinoma. Qualitative features of ccRCC including ill-defined tumor margins, calcifications, and renal vein invasion have been reported to correlate with mutations in BRCA1-associated protein 1 (BAP-1), which is known to be associated with high-grade ccRCC [39,40]. Jamshidi et al [42] reported the construction of a predictive image phenotype-based system, using 28 imaging features on CT that correlate with a previously reported supervised principal component (SPC) risk score. The SPC risk score is a quantitative multigene assay consisting of 259 genes that predict poor prognosis in ccRCC. They composed a radiogenomic risk score (RRS) using 4 of the 28 traits, including the pattern of tumor necrosis, tumor transition zone, tumor-parenchyma interactions, and tumor-parenchyma interface, that demonstrated a significant association with the SPC risk score. Importantly, the RRS performed similarly to the SPC score in the differentiation of aggressive from more indolent disease in a training set and a validation cohort.

Quantitative mpMRI protocols can be used to create objective composite phenotypes of the tumor. These phenotypes can be utilized to study histologic heterogeneity (Figure 7). Co-localization of imaging features *in vivo* with pathology and molecular analysis requires however careful co-registration of patient imaging with tissue specimens. This can be

Author Manuscript Author Manuscript Author Manuscript Author Manuscript

achieved with in vivo segmentation of tumors based on imaging datasets and subsequent creation of a physical mold using state-of-the-art 3D printing technology [41]. The 3D molds are then used to orient and section the tissue specimen after surgical resection so that samples of the tumor co-localized to imaging findings can be obtained. (Figure 8)

MR Elastography is a relatively new technology that allows to quantitate the biomechanical properties of tissue (i.e. stiffness) and has been validated in the detection and estimation of liver fibrosis [43]. This technique can be also applied to assess the tissue properties in renal tumors. Of special interest is the detection of fibromuscular stroma in ccRCC. The presence of fibromuscular stroma has been reported in both low-grade tumors (*TCEB1* mutated) and high-grade tumors (without *TCEB1* mutation)[44](Figure 9).

Radiomics in the Post-treatment Assessment of RCC

In routine clinical practice, imaging is used to monitor for treatment response in patients undergoing systemic therapy. Several criteria have been produced to assess for response in the oncologic setting, such as the Response Evaluation Criteria in Solid Tumors (RECIST). However, traditional size-based response criteria do not incorporate early predictors of response, and size measurements alone may not be sufficient to assess response with antiangiogenic therapies. Additionally, a method to predict response prior to initiating therapy would be a step toward providing personalized medicine.

Assessment of tissue perfusion via ASL and DCE MRI has been evaluated as a method to predict response and outcome in patients with metastatic ccRCC. These quantitative MRI sequences depict changes in tissue perfusion early after the initiation of therapy. Treatment with tyrosine kinase inhibitors decrease vessel density of tumors on histologic analysis, and this correlate with decreases in vessel permeability on DCE analyses [45]. In patients with metastatic ccRCC receiving sorafenib, significant decrease in tumor vascular permeability on DCE MRI manifest as changes in the transfer constant K_{trans}, early changes in K_{trans} at 3–12 weeks after initiation of therapy, and decrease tumor size at 12 weeks correlated with progression-free survival [46]. In a mouse model of renal cell carcinoma, after the initiation of sorafenib, changes in tissue perfusion with ASL were detected within 3 days of therapy [31], and histopathologic findings of decreased microvascular density also correlated with decreased perfusion on ASL. In patients with metastatic RCC receiving antiangiogenic therapy, decreasing tumor blood flow on ASL seen as early as 1 month after the initiation of therapy were shown to be associated with subsequent changes in tumor size [47]. Changes in tumor perfusion can be detected by ASL 2 weeks after initiation of antiangiogenic therapy [48]

Studies have also evaluated the use of imaging features on CT to predict response to therapeutic agents. Smith et al. [49] used a custom postprocessing software and algorithm to develop a novel system to quantify changes in the amount of vascularized tumor within specific attenuation thresholds, termed the vascular tumor burden (VTB). This semiautomated biomarker, in addition to other tumor metrics, such as length, area, and mean attenuation, were used to predict response to antiangiogenic therapy with sunitinib. Changes in the VTB metric on initial posttherapy imaging after the initiation of sunitinib showed a better separation of progression free survival between non-responders and responders

Author Manuscript Author Manuscript Author Manuscript Author Manuscript

compared to other commonly used response criteria changes in tumor metrics, including length, area, mean attenuation, RECIST, CHOI, modified CHOI, MASS, and 10% sum long diameter. Goh et al also used textural analysis on CT imaging to assess for treatment response after two cycles of treatment on a tyrosine kinase inhibitor. Using arterial phase images, ROIs were placed on CT images on all metastases at baseline and after two cycles of treatment to calculate absolute and percentage changes in image entropy and uniformity. Both baseline entropy and uniformity were significantly correlated with time to progression. Additionally, the percent change in uniformity was found to be an independent predictor of time to progression [50] .

Conclusion

Renal cell carcinoma (RCC) exhibits a heterogeneous disease spectrum, which may confound patient management and accurate image interpretation. Semi-quantitative and quantitative analysis of MRI data can aid in the characterization of this disease. Quantitative MRI acquisitions and radiomic analysis provides a method to address heterogeneity for better tumor characterization. Extension of radiomic analysis through radiogenomics, radiometabolomics, and correlation with other epidemiological, clinical and tissue-based datasets, has the potential to improve patient management in the era of personalized medicine. Understanding what these technologies can offer will allow radiologists to play a larger role in the care of patients with RCC.

Acknowledgements:

This manuscript was supported by NIH Grant P50CA196516 (I. Pedrosa, P. Kapur) and R01CA154475 (I. Pedrosa).

References

1. Weikert S, Ljungberg B. Contemporary epidemiology of renal cell carcinoma: perspectives of primary prevention. World journal of urology. 2010;28(3):247–252. [PubMed: 20390283]
2. Durinck S, Stawiski EW, Pavia-Jimenez A, et al. Spectrum of diverse genomic alterations define non-clear cell renal carcinoma subtypes. Nature genetics. 2015;47(1):13–21. [PubMed: 25401301]
3. Gerlinger M, Rowan AJ, Horswell S, et al. Intratumor Heterogeneity and Branched Evolution Revealed by Multiregion Sequencing. New Engl J Med. 2012;366(10):883–892. [PubMed: 22397650]
4. Gillies RJ, Kinahan PE, Hricak H. Radiomics: Images Are More than Pictures, They Are Data. Radiology. 2016;278(2):563–577. [PubMed: 26579733]
5. Aerts H Data Science in Radiology: A Path Forward. Clin Cancer Res. 2018;24(3):532–534. [PubMed: 29097379]
6. Mackin D, Fave X, Zhang L, et al. Measuring Computed Tomography Scanner Variability of Radiomics Features. Invest Radiol. 2015;50(11):757–765. [PubMed: 26115366]
7. Yang X, Knopp MV. Quantifying tumor vascular heterogeneity with dynamic contrast-enhanced magnetic resonance imaging: a review. J Biomed Biotechnol. 2011;2011:732848. [PubMed: 21541193]
8. Buckler AJ, Bresolin L, Dunnick NR, Sullivan DC. A collaborative enterprise for multi-stakeholder participation in the advancement of quantitative imaging. Radiology. 2011;258(3):906–914. [PubMed: 21339352]
9. Chang YC, Ackerstaff E, Tschudi Y, et al. Delineation of Tumor Habitats based on Dynamic Contrast Enhanced MRI. Sci Rep. 2017;7(1):9746. [PubMed: 28851989]

Author Manuscript Author Manuscript Author Manuscript Author Manuscript

10. Rios Velazquez E, Aerts HJ, Gu Y, et al. A semiautomatic CT-based ensemble segmentation of lung tumors: comparison with oncologists' delineations and with the surgical specimen. Radiotherapy and oncology : journal of the European Society for Therapeutic Radiology and Oncology. 2012;105(2):167–173. [PubMed: 23157978]
11. Larue RT, Defraene G, De Ruysscher D, Lambin P, van Elmpt W. Quantitative radiomics studies for tissue characterization: a review of technology and methodological procedures. The British journal of radiology. 2017;90(1070):20160665. [PubMed: 27936886]
12. Lubner MG, Smith AD, Sandrasegaran K, Sahani DV, Pickhardt PJ. CT Texture Analysis: Definitions, Applications, Biologic Correlates, and Challenges. Radiographics. 2017;37(5):1483–1503. [PubMed: 28898189]
13. Haralick RM, Shanmugam K, Dinstein I. Textural Features for Image Classification. IEEE Transactions on Systems, Man, and Cybernetics. 1973;SMC-3(6):610–621.
14. Sun MR, Ngo L, Genega EM, et al. Renal cell carcinoma: dynamic contrast-enhanced MR imaging for differentiation of tumor subtypes--correlation with pathologic findings. Radiology. 2009;250(3):793–802. [PubMed: 19244046]
15. Young JR, Coy H, Kim HJ, et al. Performance of Relative Enhancement on Multiphasic MRI for the Differentiation of Clear Cell Renal Cell Carcinoma (RCC) From Papillary and Chromophobe RCC Subtypes and Oncocytoma. AJR American journal of roentgenology. 2017;208(4):812–819. [PubMed: 28125273]
16. Wang H, Cheng L, Zhang X, et al. Renal cell carcinoma: diffusion-weighted MR imaging for subtype differentiation at 3.0 T. Radiology. 2010;257(1):135–143. [PubMed: 20713607]
17. Campbell N, Rosenkrantz AB, Pedrosa I. MRI phenotype in renal cancer: is it clinically relevant? Top Magn Reson Imaging. 2014;23(2):95–115. [PubMed: 24690616]
18. Zhang J, Pedrosa I, Rofsky NM. MR techniques for renal imaging. Radiol Clin North Am. 2003;41(5):877–907. [PubMed: 14521200]
19. Sasiwimonphan K, Takahashi N, Leibovich BC, Carter RE, Atwell TD, Kawashima A. Small (<4 cm) renal mass: differentiation of angiomyolipoma without visible fat from renal cell carcinoma utilizing MR imaging. Radiology. 2012;263(1):160–168. [PubMed: 22344404]
20. Lassel EA, Rao R, Schwenke C, Schoenberg SO, Michaely HJ. Diffusion-weighted imaging of focal renal lesions: a meta-analysis. European radiology. 2014;24(1):241–249. [PubMed: 24337912]
21. Taouli B, Thakur RK, Mannelli L, et al. Renal lesions: characterization with diffusion-weighted imaging versus contrast-enhanced MR imaging. Radiology. 2009;251(2):398–407. [PubMed: 19276322]
22. Gaing B, Sigmund EE, Huang WC, et al. Subtype differentiation of renal tumors using voxel-based histogram analysis of intravoxel incoherent motion parameters. Investigative radiology. 2015;50(3):144–152. [PubMed: 25387050]
23. Chandarana H, Rosenkrantz AB, Mussi TC, et al. Histogram analysis of whole-lesion enhancement in differentiating clear cell from papillary subtype of renal cell cancer. Radiology. 2012;265(3):790–798. [PubMed: 23175544]
24. Lubner MG, Stabo N, Abel EJ, Del Rio AM, Pickhardt PJ. CT Textural Analysis of Large Primary Renal Cell Carcinomas: Pretreatment Tumor Heterogeneity Correlates With Histologic Findings and Clinical Outcomes. AJR American journal of roentgenology. 2016;207(1):96–105. [PubMed: 27145377]
25. Schieda N, Thornhill RE, Al-Subhi M, et al. Diagnosis of Sarcomatoid Renal Cell Carcinoma With CT: Evaluation by Qualitative Imaging Features and Texture Analysis. AJR American journal of roentgenology. 2015;204(5):1013–1023. [PubMed: 25905936]
26. Korfiatis P, Kline TL, Coufalova L, et al. MRI texture features as biomarkers to predict MGMT methylation status in glioblastomas. Med Phys. 2016;43(6):2835–2844. [PubMed: 27277032]
27. Mertz KD, Demichelis F, Kim R, et al. Automated immunofluorescence analysis defines microvessel area as a prognostic parameter in clear cell renal cell cancer. Human pathology. 2007;38(10):1454–1462. [PubMed: 17889675]
28. Iakovlev VV, Gabril M, Dubinski W, et al. Microvascular density as an independent predictor of clinical outcome in renal cell carcinoma: an automated image analysis study. Laboratory

Author Manuscript Author Manuscript Author Manuscript Author Manuscript

investigation; a journal of technical methods and pathology. 2012;92(1):46–56. [PubMed: 22042086]

29. Noguchi T, Yoshiura T, Hiwatashi A, et al. Perfusion imaging of brain tumors using arterial spin-labeling: correlation with histopathologic vascular density. AJNR American journal of neuroradiology. 2008;29(4):688–693. [PubMed: 18184842]
30. Yuan Q, Kapur P, Zhang Y, et al. Intratumor Heterogeneity of Perfusion and Diffusion in Clear Cell Renal Cell Carcinoma: Correlation with Tumor Cellularity. Clinical genitourinary cancer. 2016;14(6):e585–594. [PubMed: 27209349]
31. Schor-Bardach R, Alsop DC, Pedrosa I, et al. Does Arterial Spin-labeling MR Imaging–measured Tumor Perfusion Correlate with Renal Cell Cancer Response to Antiangiogenic Therapy in a Mouse Model? Radiology. 2009;251(3):731–742. [PubMed: 19474376]
32. Zhang Y, Kapur P, Yuan Q, et al. Tumor Vascularity in Renal Masses: Correlation of Arterial Spin-Labeled and Dynamic Contrast-Enhanced Magnetic Resonance Imaging Assessments. Clinical genitourinary cancer. 2016;14(1):e25–36. [PubMed: 26422014]
33. Horiguchi A, Asano T, Asano T, Ito K, Sumitomo M, Hayakawa M. Fatty acid synthase over expression is an indicator of tumor aggressiveness and poor prognosis in renal cell carcinoma. J Urol. 2008;180(3):1137–1140. [PubMed: 18639282]
34. von Roemeling CA, Marlow LA, Wei JJ, et al. Stearoyl-CoA desaturase 1 is a novel molecular therapeutic target for clear cell renal cell carcinoma. Clin Cancer Res. 2013;19(9):2368–2380. [PubMed: 23633458]
35. Reeder SB, McKenzie CA, Pineda AR, et al. Water-fat separation with IDEAL gradient-echo imaging. J Magn Reson Imaging. 2007;25(3):644–652. [PubMed: 17326087]
36. Zhang Y, Udayakumar D, Cai L, et al. Addressing metabolic heterogeneity in clear cell renal cell carcinoma with quantitative Dixon MRI. JCI insight. 2017;2(15).
37. Saito K, Arai E, Maekawa K, et al. Lipidomic Signatures and Associated Transcriptomic Profiles of Clear Cell Renal Cell Carcinoma. Sci Rep. 2016;6:28932. [PubMed: 27357243]
38. Rosenkrantz AB, Niver BE, Fitzgerald EF, Babb JS, Chandarana H, Melamed J. Utility of the apparent diffusion coefficient for distinguishing clear cell renal cell carcinoma of low and high nuclear grade. AJR American journal of roentgenology. 2010;195(5):W344–351. [PubMed: 20966299]
39. Shinagare AB, Vikram R, Jaffe C, et al. Radiogenomics of clear cell renal cell carcinoma: preliminary findings of The Cancer Genome Atlas-Renal Cell Carcinoma (TCGA-RCC) Imaging Research Group. Abdominal imaging. 2015;40(6):1684–1692. [PubMed: 25753955]
40. Karlo CA, Di Paolo PL, Chaim J, et al. Radiogenomics of clear cell renal cell carcinoma: associations between CT imaging features and mutations. Radiology. 2014;270(2):464–471. [PubMed: 24029645]
41. Dwivedi DK, Chatzinoff Y, Zhang Y, et al. Development of a Patient-specific Tumor Mold Using Magnetic Resonance Imaging and 3-Dimensional Printing Technology for Targeted Tissue Procurement and Radiomics Analysis of Renal Masses. Urology. 2017.
42. Jamshidi N, Jonasch E, Zapala M, et al. The radiogenomic risk score: construction of a prognostic quantitative, noninvasive image-based molecular assay for renal cell carcinoma. Radiology 2015;277(1):114–23. [PubMed: 26402495]
43. Venkatesh SK, Yin M, Ehman RL. Magnetic resonance elastography of liver: technique, analysis, and clinical applications. J Magn Reson Imaging. 2013;37(3):544–555. [PubMed: 23423795]
44. Favazza L, Chitale DA, Barod R, et al. Renal cell tumors with clear cell histology and intact VHL and chromosome 3p: a histological review of tumors from the Cancer Genome Atlas database. Modern pathology : an official journal of the United States and Canadian Academy of Pathology, Inc 2017;30(11):1603–1612.
45. Drevs J, Muller-Driver R, Wittig C, et al. PTK787/ZK 222584, a specific vascular endothelial growth factor-receptor tyrosine kinase inhibitor, affects the anatomy of the tumor vascular bed and the functional vascular properties as detected by dynamic enhanced magnetic resonance imaging. Cancer research. 2002;62(14):4015–4022. [PubMed: 12124335]

Author Manuscript Author Manuscript Author Manuscript Author Manuscript

46. Flaherty KT, Rosen MA, Heitjan DF, et al. Pilot study of DCE-MRI to predict progression-free survival with sorafenib therapy in renal cell carcinoma. Cancer biology & therapy. 2008;7(4):496–501. [PubMed: 18219225]

47. de Bazelaire C, Alsop DC, George D, et al. Magnetic resonance imaging-measured blood flow change after antiangiogenic therapy with PTK787/ZK 222584 correlates with clinical outcome in metastatic renal cell carcinoma. Clinical cancer research : an official journal of the American Association for Cancer Research. 2008;14(17):5548–5554. [PubMed: 18765547]

48. Pedrosa I, Alsop DC, Rofsky NM. Magnetic resonance imaging as a biomarker in renal cell carcinoma. Cancer. 2009;115(10 Suppl):2334–2345. [PubMed: 19402070]

49. Smith AD, Zhang X, Bryan J, et al. Vascular Tumor Burden as a New Quantitative CT Biomarker for Predicting Metastatic RCC Response to Antiangiogenic Therapy. Radiology. 2016;281(2):484–498. [PubMed: 27603788]

50. Goh V, Ganeshan B, Nathan P, Juttla JK, Vinayan A, Miles KA. Assessment of response to tyrosine kinase inhibitors in metastatic renal cell cancer: CT texture as a predictive biomarker. Radiology. 2011;261(1):165–171. [PubMed: 21813743]

Author Manuscript Author Manuscript Author Manuscript Author Manuscript

Box 1.

List of Common Haralick Features.

Haralick Features
Angular second momentum
Contrast
Correlation
Difference entropy
Difference variance
Energy
Entropy
Homogeneity
Information measure of correlation 1
Information measure of correlation 2
Max correlation coefficient
Sum average
Sum entropy
Sum variance

Author Manuscript Author Manuscript Author Manuscript Author Manuscript

Key points:

- Radiomics encompasses various techniques for the extraction of quantitative features from imaging to improve diagnostic, prognostic, and predictive accuracy of image interpretation, but mandates requires standardization and large and well-designed databases for optimal utilization.
- Radiomics in the pre-treatment assessment of kidney cancer may provide additional insight into the subtyping and tumor biology of renal cell carcinoma.
- In the post-treatment setting, radiomics may assist in predicting a response to systemic therapy, including to antiangiogenic treatment which may not be adequately assessed with traditional size-based criteria.

Author Manuscript Author Manuscript Author Manuscript Author Manuscript

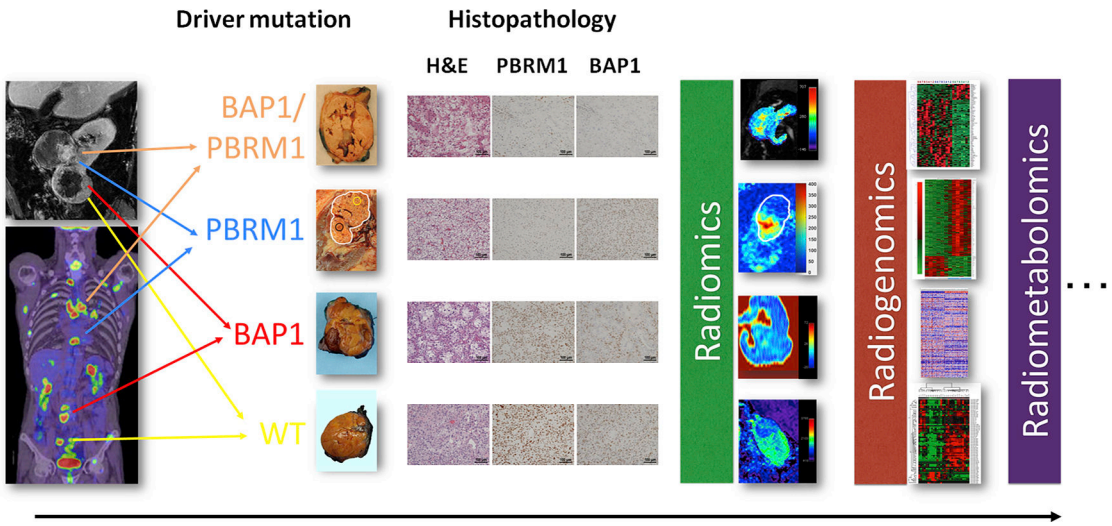

Figure 1. Schematic representation of the goal of image-based analysis in kidney cancer.

Imaging provides analysis of the entire tumor and virtually every metastatic lesion in the patient. The imaging phenotype in the primary tumor and metastatic lesions may correlate to specific underlying molecular alteration (e.g. mutation status), which can be confirmed with genomics or immunohistochemistry during histopathologic evaluation. Mining of imaging data (radiomics) offers the opportunity to correlate objective, quantitative in vivo data with datasets generated with tissue-based analyses such as histopathology, genetic data (radiogenomics), metabolomics data (radiometabolomics), and potentially others. The spatial co-localization of imaging data with tissue-based data provides an avenue to address tumor heterogeneity in kidney cancer. H&E: Haemotoxylin and Eosin. PBRM1: polybromo 1. BAP1: BRCA1-Associated Protein 1; WT, wild-type

Author Manuscript Author Manuscript Author Manuscript Author Manuscript

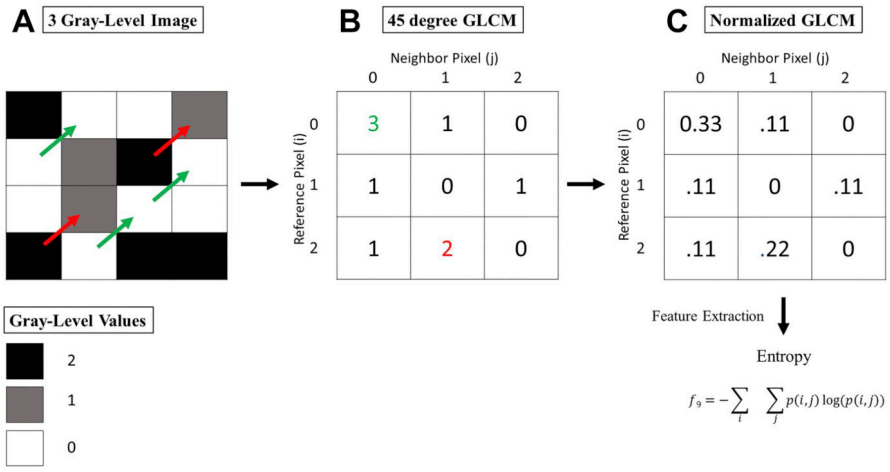

Figure 2. Example of Haralick texture features using a 3 gray level image.

In this example, a 4×4 image with 3 gray levels is assessed (A). The first step in is constructing a gray-level co-occurrence matrix (GLCM) in a specified direction (B); in this example, a 45° degree (diagonal) direction is used. The value of the reference voxel (i) establishes the appropriate row, and the value of the neighbor pixel (j) determines the column. In this example, for the reference value of 0, the co-occurrence of a neighbor pixel of 0 in the 45° degree is 3 (annotated by the green arrows), and for a reference value of 2, the co-occurrence with a neighbor pixel of 1 is 2 (annotated by the red arrows). The GLCM can then be normalized by the sum of the elements to generate a probability of each combination to occur in the image (C). Haralick statistical features can then be subsequently extracted from the region of interest.

Author Manuscript Author Manuscript Author Manuscript Author Manuscript

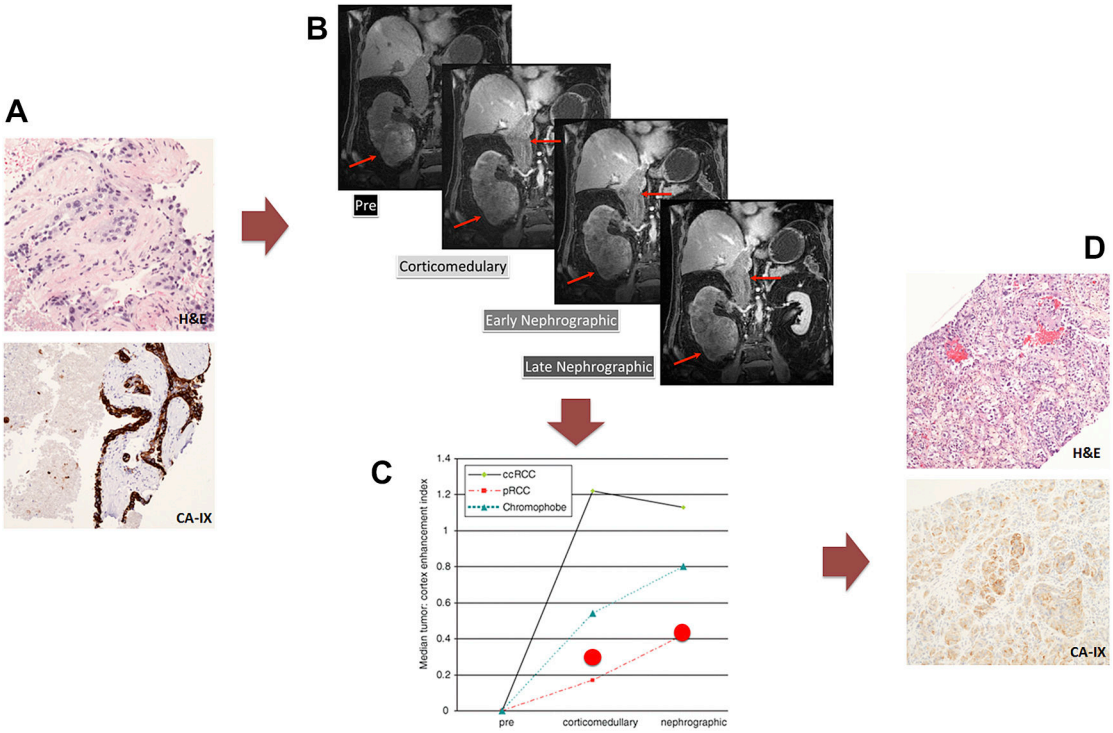

Figure 3. Use of tumor enhancement characteristics on MRI to guide treatment.

Biopsy of renal mass (A) in patient presenting with a large tumor and inferior vena cava (IVC) thrombus and synchronous pulmonary metastases. Biopsy specimen was largely necrotic with only a small foci of high grade tumor with clear cytoplasm present on hematoxylin and eosin (top) exhibiting focal positive membranous staining with CAIX (bottom). Tumor was positive for PAX8 (not shown). The possibility of clear cell RCC was considered and antiangiogenic therapy with sunitinib was recommended. MRI was performed to assess the possibility of debulking nephrectomy. Multiphasic contrast-enhanced MRI (B) showed a large right renal mass and IVC thrombus, both exhibiting very low level progressive enhancement. Quantitative analysis of renal mass enhancement relative to the renal cortex (C) was performed and found to be 35% and 42% during the corticomedullary and nephrographic phases, respectively. These enhancement characteristics would not be typical of clear cell RCC, and more suggestive of papillary histology. Based on MRI findings, a repeated biopsy was performed (D) demonstrating prominent papillary architecture (top) with microcalcifications, negative CAIX stain (bottom) and strong CK7 and racemase (not shown). Final diagnosis was high grade papillary RCC and treatment recommendation was changed to temsirolimus (Panel in C from Sun MR, Ngo L, Genega EM, et al. Renal cell carcinoma: dynamic contrast-enhanced MR imaging for differentiation of tumor subtypes--correlation with pathologic findings. Radiology. 2009 Mar;250(3):793–802, with permission).

Author Manuscript Author Manuscript Author Manuscript Author Manuscript

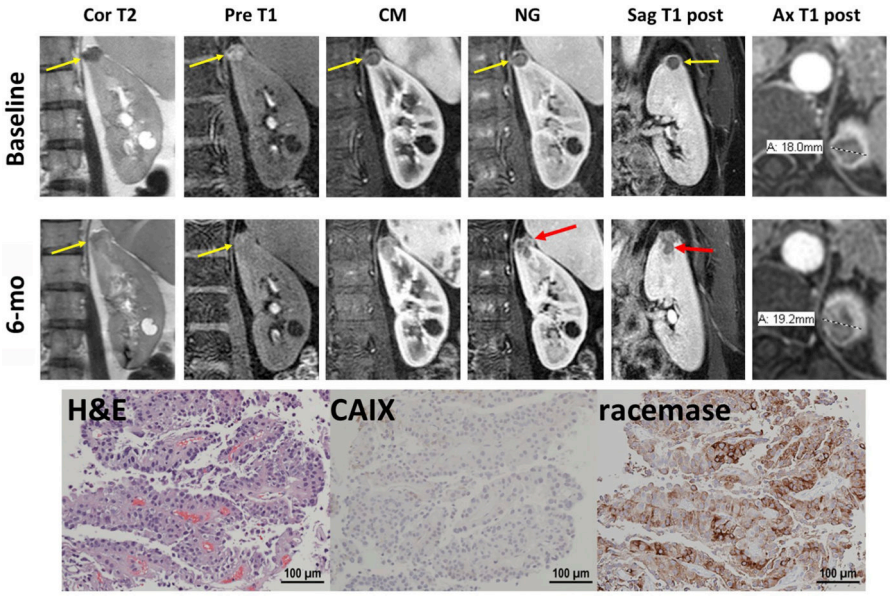

Figure 4. Aggressive behavior detected by change in imaging phenotype in small renal mass.

48-yearold female with an incidentally detected small renal mass (SRM). Baseline MRI examination (top row) shows a well encapsulated round 1.8 cm renal mass in the upper pole of the left kidney (yellow arrow) with homogeneous low signal intensity on coronal T2-weighted single shot fast spin echo image (Cor T2), high signal intensity on coronal pre-contrast T1 weighted fat saturated spoiled gradient echo images (Pre T1) and low level progressive enhancement on same images acquired during the corticomedulary (CM), early nephrographic (NG), and sagittal images during excretory phase after administration of 0.1 mmol/kg body weight of gadobutrol. MR imaging findings are consistent with papillary RCC. Ax T1 post: Axial delayed postcontrast T1-weighted. The patient remained asymptomatic and follow up MRI exam 6 months later (middle row) shows a change in signal intensity on Cor T2 and Pre-T1 images (yellow arrows). Importantly, post-contrast images demonstrate an interval change in tumor shape now infiltrating the perirenal fat (NG, red arrow) and renal parenchyma (Sag T1 post, red arrow) despite minimal change in size (1.9 cm on axial T1-weighted post contrast image). Percutaneous biopsy (bottom row) obtained prior to percutaneous ablation confirmed high grade (ISUP 3 out of 4) papillary RCC, type II. H&E: haematoxylin and eosin, CAIX: Carbonic anhydrase IX protein.

Author Manuscript Author Manuscript Author Manuscript Author Manuscript

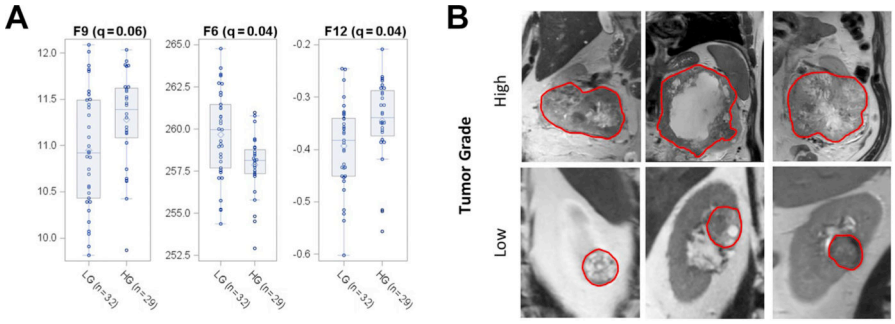

Figure 5. Extraction of MRI texture features for characterization of clear cell renal cell carcinoma.

Haralick features extracted from T2-weighted single-shot turbo spin echo (A) MRI exhibiting a statistically significant correlation with histopathologic tumor grade. LG= Low grade (ISUP grade 1–2). HG = high grade (ISUP grade 3–4). F6 = sum average. F9 = entropy. F12 = Information measures of correlation. Representative examples of tumors with high and low entropy on T2-weighted images (B) and high and low tumor grade at histopathology. q= false discovery rate.

Author Manuscript Author Manuscript Author Manuscript Author Manuscript

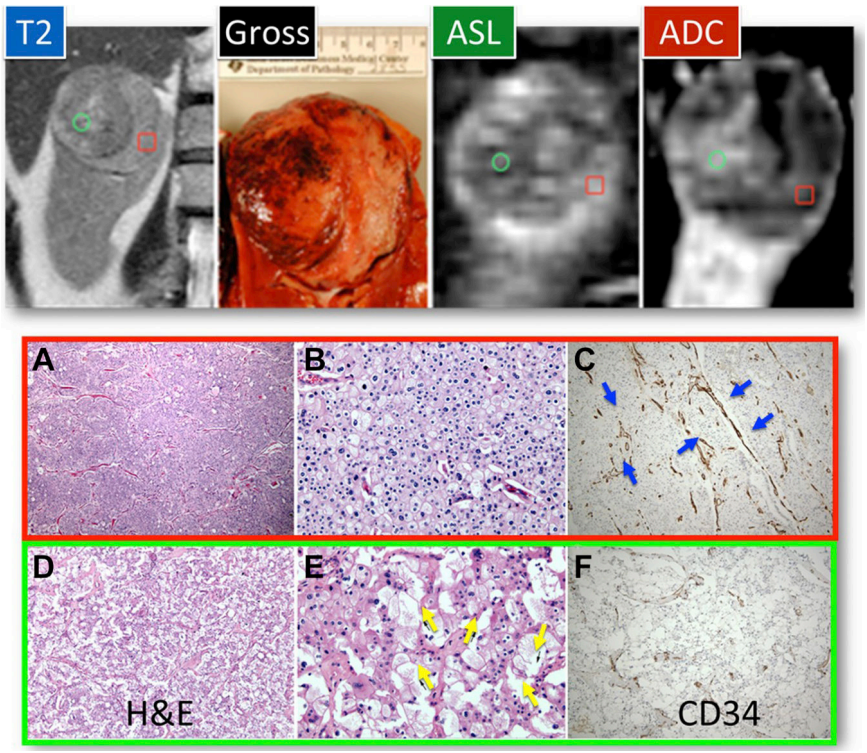

Figure 6. Quantitative MRI techniques for evaluation of tumor microenvironment in chromophobe renal cell carcinoma.

Coronal T2-weighted single-shot turbo spin echo (T2), gross specimen sectioned in the same anatomic plane after nephrectomy (gross image), and corresponding coronal ASL perfusion map and ADC map in the same location of the tumor are shown in the top panel. The bottom panel shows low (A,D; 10x) and high (B,E; 200x) magnification hematoxylin and eosin (H&E) stains and CD34 immunohistochemistry (C,F; 200x) slides corresponding to the tumor areas indicated on the MRI by the red square (top row) and green circle (bottom row). Areas with high flow on ASL (red square) also have marked restricted diffusion (i.e. low ADC) and this correlates with increased cellularity (B) and microvascular density (blue arrows, C). In contrast, areas with low flow on ASL (green circle) have increased diffusion (i.e. high ADC) indicating increased motion of water, which is likely the result of ischemia induced damage leading to the presence of cell membrane defects (E, yellow arrows). Decreased vascularity is also noted in the same area of the tumor (F).

Author Manuscript Author Manuscript Author Manuscript Author Manuscript

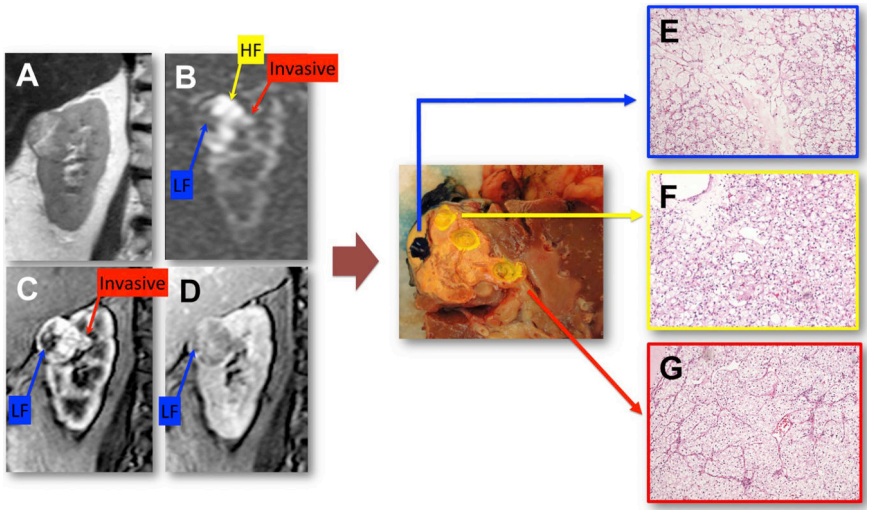

Figure 7. Multiparametric MRI as a platform to detect intra-tumor histologic heterogeneity in vivo.

Coronal T2-weighted single shot fast spin echo (A), arterial spin labeled (ASL) difference image (B), and T1-weighted gradient echo images acquired during the corticomedullary (C) and delayed (D) phases of a dynamic contrast enhanced (DCE) acquisition. After nephrectomy, tumor specimen (center panel) was sectioned with the help of fiducial markers placed during surgery in a coronal plane matching the anatomic location of the MRI images. Tumor samples were obtained in areas co-localized to regions of high flow (HF), low flow (LF), and invasive component on MRI. Histopathologic analysis of these samples revealed clear cell renal cell carcinoma (ISUP grade 3). Note differences in tumor architecture; small acinar pattern with more hyalinized stroma in the LF region (E), prototypical (“classic”) ccRCC with a small acinar pattern and thin arborizing vasculature in the high flow region (F), and a different trabecular pattern in the invasive area (G).

Author Manuscript Author Manuscript Author Manuscript Author Manuscript

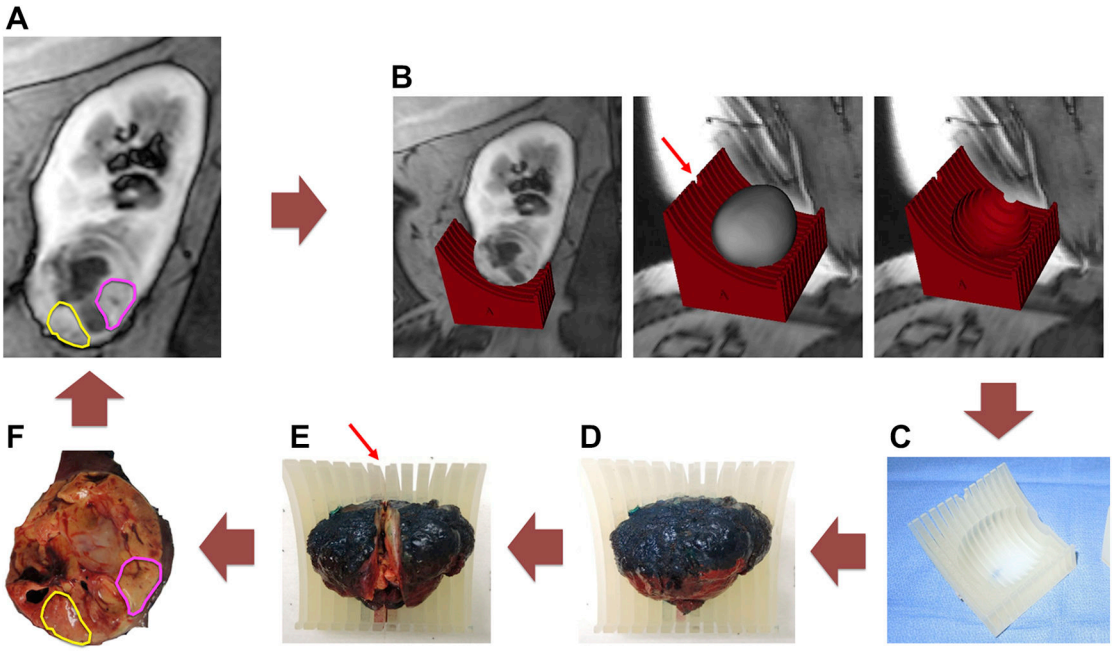

Figure 8. Registration of imaging and pathology specimens for radiogenomic analysis.

(A) Coronal contrast-enhanced three-dimensional (3D) gradient echo image of a renal mass in the lower pole of the right kidney. (B) After segmentation of the tumor, a virtual 3D mold is created. Note an indentation in the 3D mold (arrow), corresponding to the anatomic location of the coronal MRI image displayed in A. (C) Creation of the physical mold with 3D printing technology. (D) After partial nephrectomy, the specimen is oriented and placed within the 3D mold. (E) The surgical specimen is sectioned using the indentation in the 3D mold (arrow). (F) A near perfect co-localization of the surgical specimen and MRI imaging is achieved allowing the sampling of specific areas in the tumor and subsequent correlation of tumor features on MRI with histopathology and other tissue based analysis (e.g. radiogenomics, radiometabolomics, etc).

Author Manuscript Author Manuscript Author Manuscript Author Manuscript

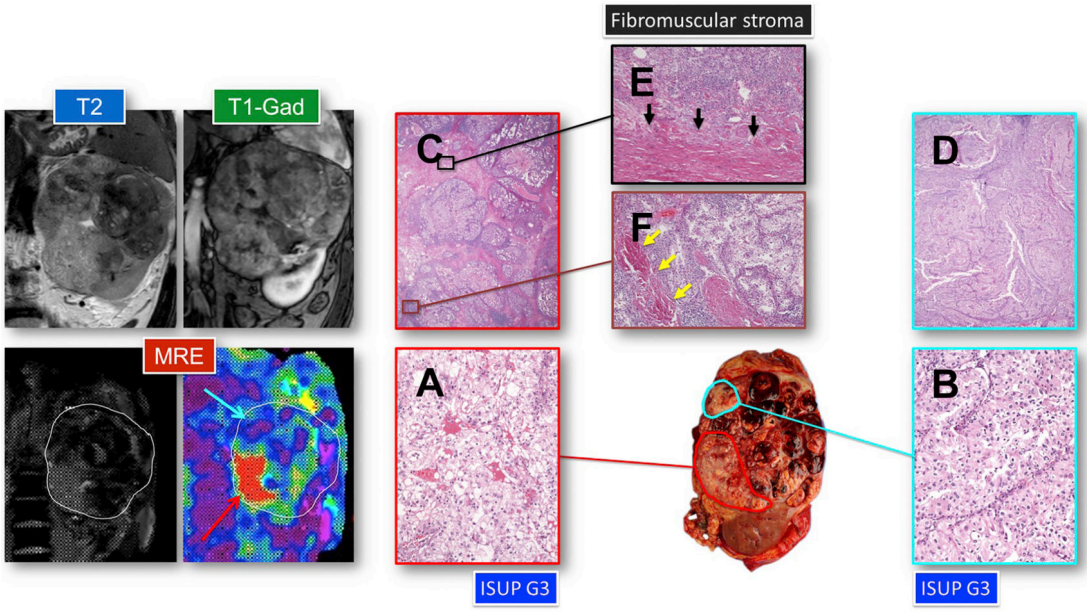

Figure 9. MR elastography (MRE) for the characterization of tissue properties in renal tumors.

Coronal T2-weighted single-shot fast spin echo image (T2) and contrast-enhanced T1-weighted gradient echo image (T1-Gad) acquired during the corticomedulary phase of a dynamic contrast-enhanced acquisition and corresponding magnitude and stiffness map from an MRE acquisition performed at the same anatomic level. Note an area of increased stiffness in the lower medial aspect of the mass (red arrow) compared with a relatively softer area in the upper medial aspect of the mass (light blue arrow). After nephrectomy, tumor specimen (right panel) was sectioned with the help of fiducial markers placed during surgery in a coronal plane matching the anatomic location of the MR images. Histopathologic assessment of both areas indicated by the red and light blue regions of interest (ROIs), which correspond with the red and light blue arrows on MRE, demonstrated no obvious differences in the International Society of Urological Pathology grade (ISUP grade 3 out of 4) of clear cell carcinoma (A, B; original magnification 200). Histopathologic images at lower magnification; however, show obvious morphologic/ architectural differences between both tumor areas (C, D; original magnification 10). Detailed analysis of the tumor region within red ROI (ie, area of increased stiffness) confirms the presence of nodular fibrosis (black arrows, E; original magnification 100) and smooth muscle in the stroma (yellow arrows, F; original magnification 100). The presence of fibromuscular stroma explains the increase stiffness detected by MRE.